Reactions of Laser-Ablated Ag and Au Atoms with Carbon Monoxide: Matrix Infrared Spectra and Density Functional Calculations on $Ag(CO)_n$ (n = 2, 3), $Au(CO)_n$ (n = 1, 2) and $M(CO)_n^+$ (n = 1−4; M = Ag, Au)

Binyong Liang and Lester Andrews*

Department of Chemistry, University of Virginia, P.O. Box 400319, Charlottesville, Virginia 22904-4319

Received: May 17, 2000; In Final Form: August 2, 2000

Laser-ablated Ag and Au atoms have been reacted with CO molecules followed by condensation in excess neon at 4 K. Besides the neutral carbonyls [$Ag(CO)_n$ (n = 2, 3), $Au(CO)_n$ (n = 1, 2), $Au_2(CO)_2$], the metal carbonyl cations [$M(CO)_n^+$ (n = 1−4)] have been formed and identified. The CO concentration, isotopic substitution and CCl_4 doping experiments confirm the identification of the cationic species. Excellent agreement between observed bands and frequencies and isotopic frequency ratios from the DFT calculations support the vibrational assignments and identification of the metal carbonyl complexes.

I. Introduction

Binary transition metal carbonyls are among the earliest known[1] and most commonly encountered organometallic compounds.[2] Many industrial processes, from hydroformylation and Fischer−Tropsch synthesis to the synthesis of acetic acid and the water-gas shift reaction, employ CO as a reagent and transition metal compounds as heterogeneous or homogeneous catalysts and involve metal carbonyl intermediates.[3] Moreover, the monocarbonyls offer zeroth-order models for interpreting the chemisorption of carbon monoxide on metal surfaces.[4,5]

As noble metal compounds, silver and gold carbonyls have been studied both experimentally and theoretically.[6] Ozin et al. reported infrared and UV−visible spectra of the reaction products made by thermal metal atom co-deposition with CO in low-temperature argon, krypton and xenon matrices, and concluded that silver[7] forms mono-, di-, and tricarbonyls while gold[8] only gives mono- and dicarbonyls. Later, two groups performed matrix electron spin resonance studies of AgCO, $Ag(CO)_2$, $Ag(CO)_3$ and AuCO, and suggested that AgCO is not a chemical species in the rare gas matrix.[9−11] Although neutral silver and gold carbonyls have been synthesized in matrix samples, there are no reports of ionic carbonyls in matrix isolation. However, in superacid solutions and in the presence of counteranions, $Ag(CO)_n^+$ (n = 1−3) and $Au(CO)_n^+$ (n = 1, 2) have been synthesized.[12−15] The vibrational spectra of these cations and their neutral counterparts reveal the bonding difference between neutral and cation species. Some of these salts have also been crystallized at low temperature, and single-crystal X-ray diffraction patterns show shorter C−O bond lengths in the cations than in the CO molecule, and suggest stronger C−O bonds in the carbonyl cations. Finally, sequential bond energies of $Ag(CO)_n^+$ (n = 1−4) cations have been determined by collision-induced dissociation.[16]

As closed-shell species, both silver and gold carbonyl cations have received more theoretical attention than their neutral counterparts, which are open-shell species.[17−20] Barnes et al. reported silver mono- and dicarbonyl cation calculations and proposed an electrostatic bonding model.[17] Watanabe et al. studied the potential energy surface of $AgCO^-$ at the MP4 level, but found no bound state.[21] Veldkamp et al. reported MP2 level studies of $M(CO)_n^+$ (M = Ag, Au; n = 1−3); all of them are bound while the dicarbonyl cations have the largest binding energies.[18] To our knowledge, for neutral silver and gold carbonyls, only AgCO and AuCO have been calculated.[22,23] An extremely small binding energy (40−50 cm^{-1}) casts serious doubt on the claimed matrix observation of AgCO.

Laser ablation coupled with matrix isolation has proven to be an efficient method to stabilize metal carbonyl ionic species.[24−29] Recently, we reported a copper carbonyl investigation which also found carbonyl cations and anions in the neon matrix.[28] In this paper, we will employ the same technique to study the vibrational spectra of silver and gold carbonyls. Theoretical calculations will also be performed on the neutral, cation and anion carbonyls to expand our knowledge of these compounds.

II. Experimental and Computational Methods

The experimental method for laser ablation and matrix isolation has been described in detail previously.[30−32] Briefly, the Nd:YAG laser fundamental (1064 nm, 10 Hz repetition rate with 10 ns pulse width) was focused to irradiate rotating silver or gold (pure metal) targets. Typically, low laser power (3−5 mJ/pulse) was used, which favors the stabilization of ionic species and minimizes cluster formation. Laser-ablated metal atoms, cations and electrons were co-deposited with carbon monoxide (0.1%-0.4%) in excess neon onto a 4−5 K CsI cryogenic window at 2−4 mmol/h for 0.5−1 h. A quartz crystal microbalance was used to measure the amount of metal deposited in the matrix;[33] we estimate the metal concentration to be about 0.02%-0.03% of the neon matrix. Carbon monoxide (Matheson) and isotopic $^{13}C^{16}O$ and $^{12}C^{18}O$ (Cambridge Isotopic Laboratories) and selected mixtures were used in different experiments. Infrared spectra were recorded at 0.5 cm^{-1} resolution on a Nicolet 750 spectrometer with 0.1 cm^{-1} accuracy using a mercury cadmium telluride (MCTB) detector down to 400 cm^{-1}. Matrix samples were annealed at different temperatures, and selected samples were subjected to photolysis using a medium-pressure mercury lamp (λ > 240 nm) with the globe removed.

Density functional theory (DFT) calculations were performed on all of the proposed reaction products using the GAUSSIAN 94 program[34] and the BPW91[35] or hybrid B3LYP[36] functional.

10.1021/jp001833e CCC: $19.00
Published on Web 09/15/2000

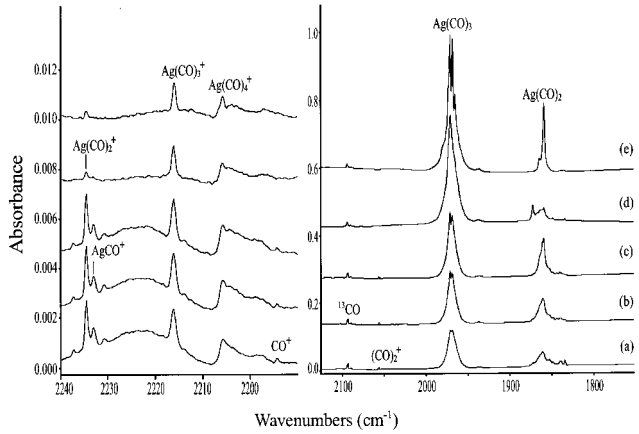

Figure 1. Infrared spectra in the 2240−2190 and 2125−1750 cm^{-1} regions for laser-ablated Ag co-deposited with 0.4% CO in neon at 4 K: (a) sample deposited for 40 min; (b) after 8 K annealing; (c) after 10 K annealing; (d) after λ > 240 nm photolysis; (e) after 12 K annealing.

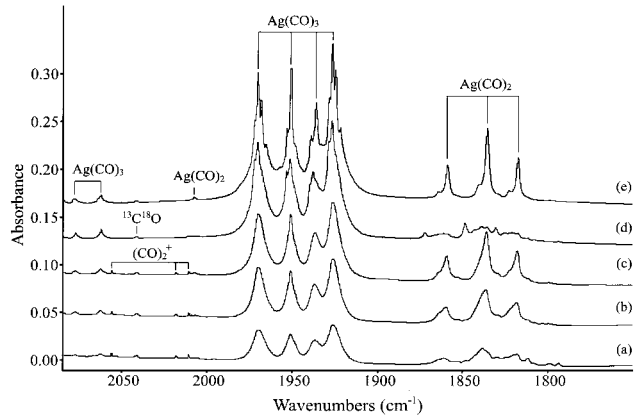

Figure 2. Infrared spectra in the 2085−1750 cm^{-1} region for laser-ablated Ag co-deposited with 0.2% ^{12}CO + 0.2% ^{13}CO in neon at 4 K: (a) sample deposited for 60 min; (b) after 8 K annealing; (c) after 10 K annealing; (d) after λ > 240 nm photolysis; (e) after 12 K annealing.

The 6-311+G* basis set was used for carbon, oxygen,[37] and the LanL2DZ effective core potential for silver and gold.[38] Basis-set superposition error (BSSE) was evaluated using the counterpoise method of Boys and Bernardi.[39] This method usually gives reasonable estimation of BSSE, although there are concerns that this method overestimates BSSE and this evaluation should be considered as an upper bound.[40]

III. Results

Infrared spectra of laser-ablated Ag and Au atom, cation and electron reaction products with CO molecules in excess neon are displayed in Figures 1−6, and the absorption bands in different isotopic experiments are listed in Tables 1 and 2. Common bands in both silver and gold experiments, also observed with copper,[28] are only listed in Table 1. These bands include a very strong CO absorption at 2140.8 cm^{-1}, its aggregate absorptions at 2159.9 and 2151.8 cm^{-1}, a weak CO^+ absorption at 2194.3 cm^{-1}, a comparatively stronger, $(CO)_2^+$ absorption at 2056.3 cm^{-1}, and $(CO)_2^-$ at 1517.5 cm^{-1}.[28,41] The metal dependent product bands and their isotopic counterparts are listed in Tables 1 and 2 for silver and gold, respectively; their behavior in different experiments and assignments will be described in the next section.

The results of DFT computations on related species are listed in the Tables 3−5. For metal mono- and dicarbonyl species

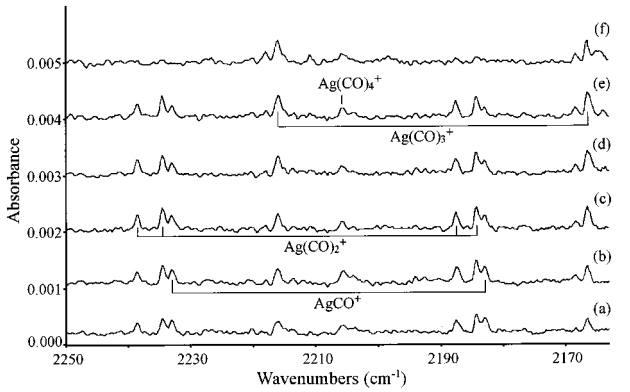

Figure 3. Infrared spectra in the 2250−2163 cm^{-1} region for laser-ablated Ag co-deposited with 0.2% ^{12}CO + 0.2% ^{13}CO in neon at 4 K: (a) sample deposited for 50 min; (b) after 8 K annealing; (c) after 10 K annealing; (d) after 11 K annealing (e) after 12 K annealing; (f) after λ > 240 nm photolysis.

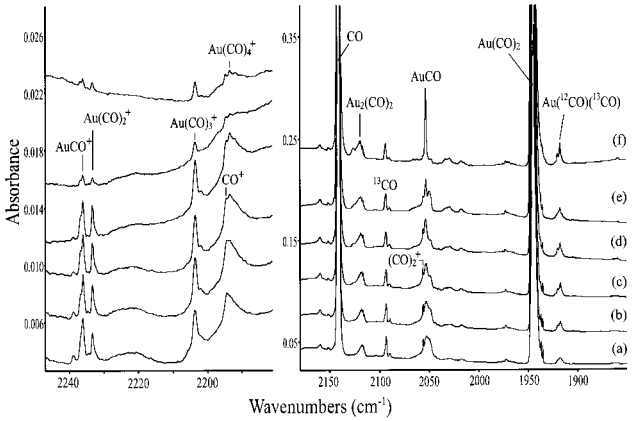

Figure 4. Infrared spectra in the 2245−2180 and 2180−1850 cm^{-1} regions for laser-ablated Au co-deposited with 0.4% CO in neon at 4 K: (a) sample deposited for 40 min; (b) after 8 K annealing; (c) after 10 K annealing; (d) after 11 K annealing; (e) after λ > 240 nm photolysis; (f) after 12 K annealing.

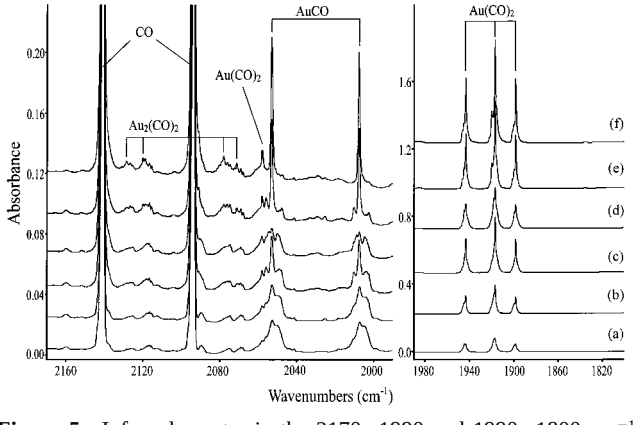

Figure 5. Infrared spectra in the 2170−1990 and 1990−1800 cm^{-1} regions for laser-ablated Au co-deposited with 0.1% ^{12}CO + 0.1% ^{13}CO in neon at 4 K: (a) sample deposited for 40 min; (b) after 6 K annealing; (c) after 9 K annealing; (d) after λ > 240 nm photolysis; (e) after 10 K annealing; (f) after 12 K annealing.

(neutrals and cations), both linear and bent forms were computed, but only the most stable ones are reported. For metal tricarbonyl species, the starting symmetries include D_{3h}, C_{3v}, and C_{2v}, the converged geometries of all the tricarbonyl species are essentially D_{3h} as listed. For metal tetracarbonyl cations, the starting symmetries include T_d, C_{3v} and D_{2d}, and both C_{3v} and D_{2d} symmetries converge to essentially T_d. Different spin

TABLE 1: Infrared Absorptions (cm^{-1}) from Reaction of Laser Ablated Ag Atoms with CO in Excess Neon at 4 K

$^{12}C^{16}O$	$^{13}C^{16}O$	$^{12}C^{18}O$	$^{13}C^{16}O + {}^{13}C^{16}O$	*R*(12/13)	*R*(16/18)	assignment
2234.6	2184.3	2183.0	2234.6, 2184.3, 2187.6, 2238.6 (sym)	1.0230	1.0236	$Ag(CO)_2^+$
2233.1	2182.9	2181.3	2233.1, 2182.9	1.0230	1.0237	$AgCO^+$
2216.0	2166.5	2164.4		1.0228	1.0238	$Ag(CO)_3^+$
2205.7	2156.6	2154.1		1.0228	1.0240	$Ag(CO)_4^+$
2194.3				1.0226	1.0225	CO^+
2159.9	2112.6	2108.8	2159.8, 2112.5	1.0224	1.0242	CO aggregate
2151.8	2104.4	2100.9	2151.8, 2104.4	1.0225	1.0242	CO aggregate
2140.8	2093.6	2089.7	2141.1, 2093.6	1.0225	1.0245	CO
2056.3	2010.9	2007.4	2056.3, 2018.4, 2010.9	1.0226	1.0244	$(CO)_2^+$
1970.4	1927.1	1925.0	1970.3, 1951.2, 1936.7, 1926.7, 2077.5 (sym), 2062.7 (sym)	1.0225	1.0236	$Ag(CO)_3$
1872.1	1830.5	1828.4	1872.1, 1848.5, 1830.5, 2011.1 (sym)	1.0227	1.0239	$Ag(CO)_2$ site
1858.7	1817.6	1815.7	1859.0, 1835.7, 1817.6, 2007.6 (sym)	1.0226	1.0237	$Ag(CO)_2$
1517.5	1484.2	1481.3	1517.5, 1499.4, 1484.2	1.0224	1.0244	$(CO)_2^-$
1516.4	1483.0	1480.4	1516.4, 1498.3, 1483.0	1.0225	1.0243	$(CO)_2^-$ site

TABLE 2: Infrared Absorptions (cm^{-1}) from Reaction of Laser Ablated Au Atoms with CO in Excess Neon at 4 K

$^{12}C^{16}O$	$^{13}C^{16}O$	$^{12}C^{18}O$	$^{13}C^{16}O + {}^{13}C^{16}O$	*R*(12/13)	*R*(16/18)	assignment
2238.9	2187.2	2189.2	2239.0, 2187.2	1.0236	1.0227	$AuCO^+$ site
2236.8	2185.3	2187.0	2236.7, 2185.2	1.0236	1.0228	$AuCO^+$
2233.4	2182.9	2182.0	2233.3, 2196.1, 2182.9, 2253.8 (sym)	1.0231	1.0236	$Au(CO)_2^+$
2203.5	2154.0	2152.5	2203.5, 2165.0, - -, 2154.0	1.0230	1.0237	$Au(CO)_3^+$
2193.5						$Au(CO)_4^+$
2118.0	2070.4	2068.8	2118.0, 2077.9, 2070.4, 2128.6 (sym)	1.0230	1.0238	$Au_2(CO)_2$ site
2116.6	2069.2	2067.5	2116.6, 2076.0, 2069.2, 2126.6 (sym)	1.0229	1.0237	$Au_2(CO)_2$
2115.4	2068.0	2066.3	2115.4, 2074.6, 2068.0, 2125.3 (sym)	1.0229	1.0238	$Au_2(CO)_2$ site
2053.2	2007.5	2004.7	2053.2, 2007.6	1.0228	1.0242	AuCO
2048.1	2003.0	1999.9	2048.2, 2002.9	1.0225	1.0241	AuCO site
1943.7	1898.5	1902.1	1943.7, 1917.0, 1898.5, 2058.1 (sym)	1.0238	1.0219	$Au(CO)_2$

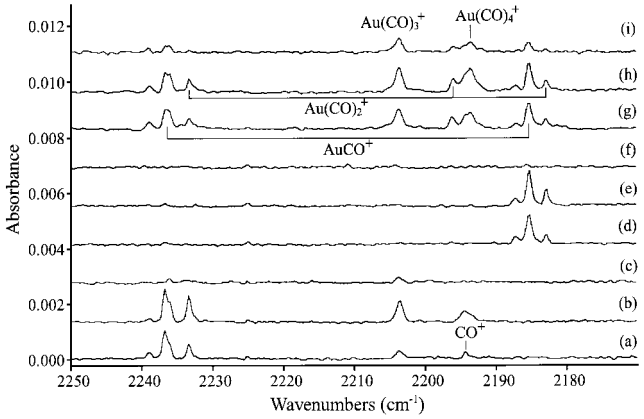

Figure 6. Infrared spectra in the 2250−2170 cm^{-1} region for laser-ablated Au co-deposited with (a, b, c) 0.2% ^{12}CO, (d, e, f) 0.1% ^{13}CO, and (g, h, i) 0.15% ^{12}CO + 0.15% ^{13}CO in neon at 4 K: (a, d, g) sample deposited for 40 min; (b, e, h) after 8 K annealing; (c, f, i) after $\lambda > 240$ nm photolysis.

states are attempted for selected molecules, and as expected, the most stable spin states are doublet and singlet for carbonyl neutrals and cations, respectively.

IV. Discussion

$Ag(CO)_n$ (n = 2, 3). Two strong absorptions observed at 1970.4 and 1858.7 cm^{-1} on deposition increase during annealings (Figure 1), and the higher CO concentration experiments favor the formation of the 1970.4 cm^{-1} band. In $^{13}C^{16}O$ and $^{12}C^{18}O$ experiments, the 1858.7 cm^{-1} band has isotopic counterparts at 1817.6 and 1815.7 cm^{-1} with isotopic ratios of 1.0225 and 1.0236, while the 1970.4 cm^{-1} band has isotopic counterparts at 1927.1 and 1925.0 cm^{-1} with similar isotopic ratios of 1.0226 and 1.0237. In the mixed $^{12}CO/^{13}CO$ experiments, the 1858.7 cm^{-1} band shows a 1:2:1 triplet feature with an intermediate band at 1835.7 cm^{-1} (Figure 2). Another new band at 2007.6 cm^{-1} is observed in the mixed isotopic experiment and tracks with the triplet. The 1858.7 cm^{-1} band is assigned to the antisymmetric C−O stretching mode of $Ag(CO)_2$. The 2007.6 cm^{-1} band is the symmetric C−O stretching mode of the $Ag(^{12}CO)(^{13}CO)$ molecule where interaction between the symmetric and antisymmetric C−O stretching modes is allowed because of symmetry breaking. The result of this interaction not only increases the intensity of the symmetric stretching mode of $Ag(^{12}CO)(^{13}CO)$ but also red shifts the antisymmetric stretching mode by 2.6 cm^{-1} from the $Ag(^{12}CO)_2-Ag(^{13}CO)_2$ median. The 1970.4 cm^{-1} band shows a quartet splitting pattern in the mixed $^{12}CO/^{13}CO$ experiment with intermediate bands at 1951.2 and 1936.7 cm^{-1} (in Figure 2, the intensity ratio is 5:4:3:6 owing to slightly more ^{13}CO than ^{12}CO). This band is assigned to the doubly degenerate C−O stretching mode[42] of $Ag(CO)_3$. Similar to the $Ag(CO)_2$ molecule, two mixed isotopic bands for the symmetric C−O stretching mode are also observed in the $^{12}CO + {}^{13}CO$ isotopic experiment at 2077.5 and 2062.7 cm^{-1} (Figure 2). The present neon matrix bands are blue shifted 15 and 17 cm^{-1} from the previous[7] argon matrix observations for $Ag(CO)_2$ and $Ag(CO)_3$.

In our Ne matrix experiment, no evidence of the isolated silver monocarbonyl is found. Earlier researchers claimed the existence of the monocarbonyl in Ar, Kr, and Xe matrices.[7] However, later experimental[9] and theoretical[22] studies have questioned the existence of the isolated silver monocarbonyl. In the argon matrix ESR study, Kasai et al. found for AgCO the spin density in the Ag 5s orbital is 0.99, and the ^{13}C hyperfine interaction is of the magnitude expected for "Ag atoms" substitutionally incorporated in the matrix separated from CO by the nearest-neighbor distance of the host lattice.[9] This result suggests that AgCO is not a bona fide complex, and that the infrared absorption at 1958 cm^{-1} in argon assigned to AgCO is questionable since the large red-shift (180 cm^{-1}) compared to isolated CO suggests strong bonding between Ag and CO.

DFT calculations have been performed on silver carbonyls. The ground state of silver monocarbonyl is found to be $^2A'$, a bent molecule. The ground states of silver di- and tricarbonyls

TABLE 3: Ground Electronic States, Equilibrium Geometries, Dissociation Energies, and Frequencies Calculated for the Ag Carbonyls[a]

species	elec state	point group	D_e (kcal/mol)[b]	D_0 (kcal/mol)[b]	D_0' (kcal/mol)[b]	geometry (Å, deg)	frequencies (intensity)[d]
				B3LYP			
CO	$^1\Sigma^+$	$C_{\infty v}$				C−O: 1.128	2211.8 (89)
AgCO	$^2A'$	C_s	0.9	0.7	−0.2	Ag−C: 2.636 C−O: 1.133 ∠AgCO: 125.4	44.9 (1), 163.7 (7), 2130.4 (631)
$Ag(CO)_2$	$^2A_1$	C_{2v}	2.4	1.7	0.7	Ag−C: 2.276 C−O: 1.142 ∠CAgC: 172.8 ∠AgCO: 136.6	217.4 (7), 291.1 (29), 1999.2 (4108), 2082.2 (8)
$Ag(CO)_3$	$^2A_2''$	D_{3h}	1.4	−0.2	−1.2	Ag−C: 2.147 C−O: 1.139	247.8 (0), 319.7 (0 × 2), 2024.8 (3521 × 2), 2143.3 (0)
$AgCO^+$	$^1\Sigma^+$	$C_{\infty v}$	21.7[c]	20.6	20.3	Ag−C: 2.232 C−O: 1.116	217.0 (0 × 2), 220.7 (0), 2314.8 (77)
$Ag(CO)_2^+$	$^1\Sigma_g^+$	$D_{\infty h}$	24.9	23.3	22.4	Ag−C: 2.170 C−O: 1.116	276.0 (0 × 2), 291.0 (1), 2313.9 (231), 2321.6 (0)
$Ag(CO)_3^+$	$^1A_1'$	D_{3h}	8.3	7.9	7.4	Ag−C: 2.294 C−O: 1.118	233.3 (0), 246.8 (0 × 2), 2291.0 (163 × 2), 2298.0 (0)
$Ag(CO)_4^+$	$^1A_1$	T_d	7.0	6.4	5.7	Ag−C: 2.377 C−O: 1.119	215.3 (1 × 3), 2280.9 (138 × 3), 2288.2 (0)
				BPW91			
CO	$^1\Sigma^+$	$C_{\infty v}$				C−O: 1.139	2128.1 (75)
AgCO	$^2A'$	C_s	4.0	3.6	2.3	Ag−C: 2.273 C−O: 1.153 ∠AgCO: 128.9	148.8 (3), 260.8 (8), 1984.5 (856)
$Ag(CO)_2$	$^2A_1$	C_{2v}	9.1	8.0	6.6	Ag−C: 2.107 C−O: 1.159 ∠CAgC: 176.4 ∠AgCO: 147.9	259.9 (1), 374.1 (24), 1923.7 (2991), 2002.5 (0)
$Ag(CO)_3$	$^2A_2''$	D_{3h}	5.4	4.0	2.9	Ag−C: 2.102 C−O: 1.152	267.6 (0), 345.2 (0 × 2), 1972.8 (2289 × 2), 2061.5 (0)
$AgCO^+$	$^1\Sigma^+$	$C_{\infty v}$	24.3[c]	23.2	23.0	Ag−C: 2.157 C−O: 1.128	219.3 (0 × 2), 250.6 (1), 2221.8 (92)
$Ag(CO)_2^+$	$^1\Sigma_g^+$	$D_{\infty h}$	27.6	26.0	24.9	Ag−C: 2.120 C−O: 1.127	281.7 (0 × 2), 304.9 (7), 2221.0 (273), 2234.5 (0)
$Ag(CO)_3^+$	$^1A_1'$	D_{3h}	8.5	8.0	7.4	Ag−C: 2.224 C−O: 1.130	249.7(0), 273.6 (0 × 2), 2197.3 (205 × 2), 2208.5(0)
$Ag(CO)_4^+$	$^1A_1$	T_d	6.9	6.3	5.6	Ag−C: 2.297 C−O: 1.131	239.5 (1 × 3), 2185.6 (171 × 3), 2197.1 (0)

[a] DFT calculation: B3LYP or BPW91 functional, 6-311+G* basis set on C and O, LANL2DZ basis set and ECP on Ag. The ground state of Ag atom is calculated as $[Kr]4d^{10}5s^1$ configuration. [b] Dissociation energies refer to reactions: $Ag(CO)_n^q \rightarrow Ag(CO)_{n-1}^q + CO$. D_e is electronic energy, D_0 is electronic energy plus zero-point energy (ZPE) correction, D_0' is D_0 plus basis set superposition error (BSSE) correction. [c] Relative energy compared to AgCO (IE of AgCO) is 157.9 and 158.6 kcal/mol in B3LYP and BPW91, respectively. [d] Highest frequencies listed, no negative roots for any frequencies.

are found to be $^2A_1$ and $^2A_2''$, and possess C_{2v} and D_{3h} symmetries, respectively. Detailed geometric parameters are listed in Table 3. All three silver carbonyls are predicted to be stable with positive equilibrium dissociation energies (refer to the reactions $Ag(CO)_n \rightarrow Ag(CO)_{n-1} + CO$, $n = 1$, 2, and 3, respectively, Table 3) in both B3LYP and BPW91 calculations. A very small D_e value of AgCO (0.9 and 4.0 kcal/mol in B3LYP and BPW91, respectively) indicates its instability and justifies its absence in matrix spectroscopic studies. On the other hand, we should consider zero-point energy (ZPE) and basis set superposition error (BSSE) corrections since these are on the order of several kcal/mol. The ZPE and BSSE corrected values are also listed in Table 3. In B3LYP functional calculation, the D_0' value is negative for AgCO, however it is also negative for $Ag(CO)_3$. Efforts are made to search for another equilibrium state of $Ag(CO)_3$, but no lower states are found. While the experimental results are confirmed by several research groups, we believe that silver carbonyls present difficult theoretical problems. Finally, it should also be noted that for AgCO, especially the B3LYP functional calculation, a comparatively long Ag−C distance (2.636 D) and high C−O vibrational mode (2130.4 cm^{-1}) also indicate the weak nature of any interaction between Ag and CO.

For $Ag(CO)_2$ and $Ag(CO)_3$ the antisymmetric and doubly degenerate C−O stretching modes are predicted at 1999.2 and 2024.8 cm^{-1} (with scale factors 0.930 and 0.973) by B3LYP calculation, and 1923.7 and 1972.8 cm^{-1} (with scale factors 0.966 and 0.999) by BPW91 calculation, for $Ag(CO)_2$ and $Ag(CO)_3$, respectively. Apparently, the $Ag(CO)_2$ result does not fit with the experiment as well. Two possible reasons need to be considered. First, since the isolated silver monocarbonyl does not exist, the silver dicarbonyl only can be formed via a reaction between two CO molecules and a silver atom. This requires that two CO molecules and one silver atom coexist in a single matrix cage. In such a loose cage, the molecule is prone to be influenced by the matrix cage and may not relax to the exact ground-state geometry that the calculation predicts. This loose cage effect is also observed in our experiment; the $Ag(CO)_2$ absorption blue shifts 13.7 cm^{-1} after ultraviolet photolysis, then on the following annealing, the band returns to its original position. Ozin et al. also reported erratic frequency shifts for $Ag(CO)_2$ in Ar, Kr, and Xe matrices, indicating the elusive nature of this species.[7] Second, $Ag(CO)_2$ and $Ag(CO)_3$ are open-shell species and difficult subjects for DFT calculation. The isotopic frequency ratios calculated for these two vibrational

TABLE 4: Ground Electronic States, Equilibrium Geometries, Dissociation Energies, and Frequencies Calculated for the Au Carbonyls[a]

species	elec state	point group	D_e (kcal/mol)[b]	D_0 (kcal/mol)[b]	D_0' (kcal/mol)[b]	geometry (Å, deg)	frequencies (intensity)[d]
				B3LYP			
AuCO	$^2A'$	C_s	8.2	7.6	6.1	Au−C: 2.093 C−O: 1.141 ∠AuCO: 125.4	211.1 (15), 329.8 (6), 2065.9 (833)
$Au(CO)_2$	$^2A_1$	C_{2v}	13.0	11.5	9.6	Au−C: 1.998 C−O: 1.148 ∠CAuC: 176.9 ∠AgCO: 159.9	377.6 (0), 389.4 (57), 1981.3 (3954), 2104.2 (4)
$Au(CO)_3$	$^2A_2''$	D_{3h}	−5.2	−6.8	−7.9	Au−C: 2.028 C−O: 1.141	345.9 (0), 438.1 (5 × 2), 2045.9 (2437 × 2), 2146.4 (0)
$AuCO^+$	$^1\Sigma^+$	$C_{\infty v}$	45.9[c]	44.3	43.9	Au−C: 1.946 C−O: 1.117	325.5 (0 × 2), 391.9 (12), 313.7 (208)
$Au(CO)_2^+$	$^1\Sigma_g^+$	$D_{\infty h}$	45.7	43.9	43.0	Au−C: 2.010 C−O: 1.116	376.3 (0), 391.4 (5), 408.8 (6), 2307.4 (491), 2341.3 (0)
$Au(CO)_3^+$	$^1A_1'$	D_{3h}	−0.4	−0.8	−1.5	Au−C: 2.120 C−O: 1.119	341.6 (9), 368.7 (1 × 2), 2274.0 (340 × 2), 2294.6 (0)
$Au(CO)_4^+$	$^1A_1$	T_d	1.4	1.2	0.2	Au−C: 2.217 C−O: 1.120	301.6 (2 × 3), 2266.2 (261 × 3), 2285.6 (0)
$Au_2(CO)_2$	$^1\Sigma_g^+$	$D_{\infty h}$	65.1[e]	63.5	61.5	Au−Au: 2.568 Au−C: 2.044 C−O: 1.131	304.2 (0), 321.7 (0 × 2), 2171.4 (1118), 2186.1 (0)
				BPW91			
AuCO	$^2A'$	C_s	16.3	15.6	13.3	Au−C: 2.016 C−O: 1.157 ∠AuCO: 138.8	243.0 (16), 400.2 (4), 1973.2 (695)
$Au(CO)_2$	$^2A_1$	C_{2v}	20.1	18.6	16.1	Au−C: 1.973 C−O: 1.161 ∠CAuC: 177.3 ∠AgCO: 159.8	401.6 (0), 406.5 (26), 1944.0 (2431), 2035.5 (2)
$Au(CO)_3$	$^2A_2''$	D_{3h}	−0.3	−1.9	−3.2	Au−C: 2.003 C−O: 1.155	368.4 (0), 454.5 (8 × 2), 1985.5 (1733 × 2), 2063.5 (0)
$AuCO^+$	$^1\Sigma^+$	$C_{\infty v}$	55.4[c]	53.7	53.1	Au−C: 1.903 C−O: 1.130	330.9 (0 × 2), 439.3 (15), 2222.8 (204)
$Au(CO)_2^+$	$^1\Sigma_g^+$	$D_{\infty h}$	48.8	46.9	45.7	Au−C: 1.988 C−O: 1.128	397.9 (0), 409.4 (4 × 2), 2212.6 (510), 2254.2 (0)
$Au(CO)_3^+$	$^1A_1'$	D_{3h}	2.2	1.7	0.8	Au−C: 2.075 C−O: 1.131	362.5 (8), 397.6 (1 × 2), 2177.0 (378 × 2), 2202.0 (0)
$Au(CO)_4^+$	$^1A_1$	T_d	2.3	2.1	0.7	Au−C: 2.153 C−O: 1.132	335.4 (2 × 3), 2168.5 (308 × 3), 2193.4 (0)
$Au_2(CO)_2$	$^1\Sigma_g^+$	$D_{\infty h}$	66.7[e]	65.3	62.4	Au−Au: 2.562 Au−C: 2.002 C−O: 1.145	334.8 (0 × 2), 350.0 (0), 2077.0 (1162), 2095.5 (0)

[a] DFT calculation: B3LYP or BPW91 functional, 6-311+G* basis set on C and O, LANL2DZ basis set and ECP on Au. The ground state of Au atom is calculated as $[Xe]4f^{14}5d^{10}6s^1$ configuration. [b] Dissociation energies refer to the reactions: $Au(CO)_n^q \rightarrow Au(CO)_{n-1}^q + CO$, D_e is electronic energy, D_0 is electronic energy plus zero-point energy (ZPE) correction, D_0' is D_0 plus basis set superposition error (BSSE) correction. [c] Relative energy compared to AuCO (IE of AuCO) is 179.5 and 180.0 kcal/mol in B3LYP and BPW91, respectively. [d] Highest frequencies listed, no negative roots for any frequencies except $Au(CO)_3^+$ in B3LYP calculation and $Au(CO)_4^+$ in both calculations (see text). [e] Refer to the reaction: $Au_2(CO)_2 \rightarrow 2AuCO$.

modes are listed in Table 5, and they predict correct trends for these two modes.

$Au(CO)_n$ (n = 1, 2). Similar to silver experiments, two bands at 2053.2 and 1943.7 cm^{-1} are observed after deposition (Figure 4). In the 0.1% CO experiment, the 1943.7 cm^{-1} band is about 2 times stronger than the 2053.2 cm^{-1} band on deposition, and 10 times stronger after 8 K annealing. In the extremely low CO concentration (0.005%) experiment, the 2053.2 cm^{-1} band is about 3 times stronger than the 1943.7 cm^{-1} band after deposition, but after 8 K annealing, the 1943.7 cm^{-1} band is 2 times stronger than the 2053.2 cm^{-1} band. The 2053.2 cm^{-1} band has ^{13}CO and $C^{18}O$ counterparts at 2007.5 and 2004.7 cm^{-1}, while the 1943.7 cm^{-1} band has isotopic counterparts at 1898.5 and 1902.1 cm^{-1}. The isotopic splitting patterns of these two bands in the mixed $^{12}CO/^{13}CO$ experiment, however, are different from the silver experiment. The 2053.2 cm^{-1} band shows a doublet feature with only two pure isotopic absorptions. The 1943.7 cm^{-1} band has a 1:2:1 triplet feature with an intermediate band at 1917.0 cm^{-1} (Figure 5). On the basis of the annealing and isotopic splitting behaviors, it is clear that the absorptions at 2053.2 and 1943.7 cm^{-1} are due to the C−O stretching mode of AuCO and the antisymmetric C−O stretching mode of $Au(CO)_2$, respectively. The symmetric stretching mode of $Au(^{12}CO)(^{13}CO)$ is observed at 2058.1 cm^{-1}. This result is compatible with the previous argon[8] matrix experiment, with 13.8 and 17.1 cm^{-1} blue shifts in neon for AuCO and $Au(CO)_2$, respectively. However, no evidence is found for the $Au(CO)_3$ molecule. The previous neon matrix experiment[8] using 10% CO reported a broad $Au(CO)_2$ absorption at 1935.8 cm^{-1}, 7.9 cm^{-1} below our sharp spectrum with 0.1% CO. Clearly the previous 10% CO experiment contained $Au(CO)_2(CO)_x$ aggregates, which shows that $Au(CO)_3$ cannot be formed.

Our DFT calculations predict that gold carbonyls have the same ground states and similar geometries as the silver counterparts (Table 3). In B3LYP calculations, AuCO is predicted to be 6.1 kcal/mol (ZPE and BSSE corrected value) more stable than Au and CO, while $Au(CO)_2$ is 9.6 kcal/mol

TABLE 5: Comparison of Computed and Experimental C−O Stretching Modes of the Silver and Gold Carbonyls

		experimental			computed				scale factor
species	ν_{C-O} mode	freq (cm^{-1})	*R* (12/13)	*R* (16/18)	method	freq (cm^{-1})	*R* (12/13)	*R* (16/18)	(exp/comp)
$Ag(CO)_2$	b_2	1858.7	1.0226	1.0237	B3LYP	1999.2	1.0226	1.0251	0.930
					BPW91	1923.7	1.0230	1.0244	0.966
$Ag(CO)_3$	e′	1970.4	1.0225	1.0236	B3LYP	2024.8	1.0230	1.0244	0.973
					BPW91	1972.8	1.0233	1.0240	0.999
$AgCO^+$	σ	2233.1	1.0230	1.0237	B3LYP	2314.8	1.0232	1.0242	0.965
					BPW91	2221.8	1.0232	1.0241	1.005
$Ag(CO)_2^+$	σ_u	2234.6	1.0230	1.0236	B3LYP	2313.9	1.0233	1.0241	0.966
					BPW91	2221.0	1.0233	1.0241	1.006
$Ag(CO)_3^+$	e′	2216.0	1.0228	1.0238	B3LYP	2291.0	1.0230	1.0244	0.967
					BPW91	2197.3	1.0231	1.0231	1.009
$Ag(CO)_4^-$	t_2	2205.7	1.0228	1.0240	B3LYP	2280.9	1.0230	1.0244	0.967
					BPW91	2185.6	1.0230	1.0245	1.009
AuCO	a′	2053.2	1.0228	1.0242	B3LYP	2065.9	1.0225	1.0251	0.994
					BPW91	1973.2	1.0228	1.0248	1.041
$Au(CO)_2$	b_2	1943.7	1.0238	1.0219	B3LYP	1981.3	1.0235	1.0235	0.981
					BPW91	1944.0	1.0238	1.0233	1.000
$AuCO^+$	σ	2236.8	1.0236	1.0228	B3LYP	2313.7	1.0237	1.0234	0.967
					BPW91	2222.8	1.0241	1.0228	1.006
$Au(CO)_2^+$	σ_u	2233.4	1.0231	1.0236	B3LYP	2307.4	1.0233	1.0241	0.968
					BPW91	2212.6	1.0233	1.0240	1.009
$Au(CO)_3^+$	e′	2203.5	1.0230	1.0237	B3LYP	2274.0	1.0230	1.0244	0.969
					BPW91	2177.0	1.0231	1.0242	1.012
$Au(CO)_4^+$	t_2	2193.5			B3LYP	2266.2	1.0229	1.0245	0.968
					BPW91	2168.5	1.0230	1.0245	1.012
$Au_2(CO)_2$	σ_u	2116.6	1.0229	1.0237	B3LYP	2171.4	1.0230	1.0244	0.975
					BPW91	2077.0	1.0233	1.0241	1.019
CO	σ	2141.1	1.0227	1.0246	B3LYP	2211.8	1.0228	1.0248	0.968
					BPW91	2128.1	1.0228	1.0248	1.006
CO^+	σ	2194.3			B3LYP	2302.5	1.0228	1.0247	0.953
					BPW91	2213.2	1.0228	1.0247	0.991
$(CO)_2^+$	b_u	2056.3	1.0226	1.0244	B3LYP	2126.4	1.0228	1.0248	0.967
					BPW91	2045.9	1.0228	1.0247	1.005

more stable than AuCO and CO. However, gold tricarbonyl is 7.9 kcal/mol less stable than CO and gold dicarbonyl. Similar dissociation energies are also produced by BPW91 calculation. In previous and present low-temperature matrix studies, no evidence has been found for gold tricarbonyl.

Compared to other transition metal carbonyl studies[25,27−29] where saturated carbonyls are more stable than unsaturated carbonyls and the dominant absorptions after higher temperature annealing in the matrix experiments, the gold carbonyl system is different. Kasai et al. attributed this phenomenon to a higher 6s → 6p promotion energy for the gold atom since it is the metal p_π orbitals that give back-donation in the trigonal-planar tricarbonyls.[10] In our DFT calculation, the negative binding energy for $Au(CO)_3$ simply means the energy required to make this 6s → 6p promotion cannot be compensated by the energy lowering due to the formation of σ donation and π back-donation metal-CO bonds.

The calculated frequencies and the isotopic ratios of the observed modes are listed in the Table 4. As expected, the calculations predict correct trends for gold carbonyl vibrational modes with scale factors of 0.994 and 0.981 in B3LYP, 1.041 and 1.000 in BPW91, for modes belonging to AuCO and $Au(CO)_2$, respectively.

$Au_2(CO)_2$. The band observed at 2118.0, 2116.6, and 2115.4 cm^{-1} on deposition increases slightly during annealings, and shows no change on photolysis (Figure 4). In the ^{13}CO experiment, the band shifts to 2070.4, 2069.2, and 2068.0 cm^{-1} with an average 12/13 isotopic ratio 1.0229. In the $C^{18}O$ experiment, the band shifts to 2068.8, 2067.5, and 2066.3 cm^{-1} with an average 16/18 isotopic ratio 1.0238. In the mixed ^{12}CO and ^{13}CO experiment, two sets of new associated bands are observed besides two sets of pure ^{12}CO and ^{13}CO isotopic bands. The stronger band around 2076 cm^{-1} is between the two pure isotopic bands, while the weaker band around 2126 cm^{-1} is higher than the pure ^{12}CO band (Table 2). On the basis of the characteristic 12/13 and 16/18 isotopic ratios and splitting pattern in the mixed isotopic experiment, this band is due to a dicarbonyl species. In the 0.2% CO experiment, the $Au(CO)_2$ band is 31 times and the AuCO band is 9.4 times stronger than this band on deposition, while after 12 K annealing, the $Au(CO)_2$ band is 68 times and the AuCO band is 8.9 times stronger. In the 0.4% CO experiment, the $Au(CO)_2$ band is 31 times and the AuCO band is 2.1 times stronger than this band on deposition, while after 12 K annealing, the $Au(CO)_2$ band is 66 times and the AuCO band is 4.9 times stronger. Since this band is favored over the AuCO band by a higher CO concentration, and less favored by annealing than both AuCO and $Au(CO)_2$ bands, this band can be assigned to the antisymmetric C−O stretching mode of $Au_2(CO)_2$. The band observed at 2125.3 cm^{-1} in the mixed $^{12}CO/^{13}CO$ isotopic experiment is the symmetric C−O stretching mode of $Au_2(^{12}CO)(^{13}CO)$.

DFT calculations characterize this $Au_2(CO)_2$ molecule with $D_{\infty h}$ symmetry and a $^1\Sigma_g^+$ ground electronic state (Table 4). In the DFT/B3LYP calculation, no negative frequencies are produced. The predicted antisymmetric C−O stretching frequency is 2171.4 cm^{-1}, and the 12/13 and 16/18 isotopic ratios are 1.0230 and 1.0244. This frequency requires a 0.975 scale factor, an expected value for DFT/B3LYP calculation.[43] On the basis of relative intensities in different CO concentration experiments and on annealing, the mechanism for producing this $Au_2(CO)_2$ molecule is probably dimerization of AuCO. The binding energy of the dimerization is calculated as 65.1 kcal/mol. In BPW91 calculation, similar results are produced and the scale factor of the σ_u C−O stretching mode is 1.019. A small negative doubly degenerate bending mode found at −14.0 cm^{-1} is attributed to numerical problems.

Compared to the thermal metal reactions, laser ablation also introduces cations and electrons into the reaction system. Additional weak bands are observed in the higher C−O stretching region, above the free C−O stretching frequency, 2140.8 cm^{-1}. These bands are photosensitive, and the absorption intensities increase in the CCl_4 doping experiments. Hence, cation species must be considered.[26−29]

$Ag(CO)_n^+$ (n = 1−4). In the 0.1% CO experiment (not shown), the 2233.1 cm^{-1} band is observed on deposition, and almost does not change during annealing to 10 K, then disappears on the following full-arc photolysis. Another band at 2234.6 cm^{-1} is also observed on deposition with a similar intensity. Upon annealing to 10 K, the intensity of this 2234.6 cm^{-1} band tripled, and full-arc photolysis almost destroys this band. Since these two bands are very close to each other, more evidence is required to identify them. Several CO concentration experiments (from 0.1% to 0.4%) were performed, and they clearly show that the 2234.6 cm^{-1} band is favored by higher CO concentrations relative to the 2233.1 cm^{-1} band. The 2234.6 cm^{-1} band has $^{13}C^{16}O$ and $^{12}C^{18}O$ isotopic counterparts at 2184.3 and 2183.0 cm^{-1}, respectively, while the 2233.1 cm^{-1} band has corresponding counterparts at 2182.9 and 2181.3 cm^{-1}. In the mixed $^{12}CO/^{13}CO$ experiment (Figure 3), the 2233.1 cm^{-1} band only shows a doublet feature with two pure isotopic absorptions. The 2233.1 cm^{-1} band is assigned to the C−O stretching mode of the $AgCO^+$ cation. In the same mixed isotopic experiment, the 2234.6 cm^{-1} band shows an asymmetric triplet feature that has an intensity ratio close to 1:1:1, with the intermediate band at 2187.6 cm^{-1}, only 3.3 cm^{-1} higher than the pure ^{13}CO absorption and a new band at 2238.6 cm^{-1} that tracks with the triplet. The 2234.6 cm^{-1} band is assigned to the antisymmetric C−O stretching mode of $Ag(CO)_2^+$. It is worth noting that the asymmetric triplet feature and the associated comparatively strong symmetric C−O stretching absorption at 2238.6 cm^{-1} show a strong interaction between the symmetric and antisymmetric C−O stretching modes in the $Ag(^{12}CO)(^{13}CO)^+$ cation.

Two more bands not observed on deposition grow in during annealings in the 0.1% CO experiment. The 2216.1 cm^{-1} band can be identified after 6 K annealing while the 2205.7 cm^{-1} band can only be found after 10 K annealing. In the 0.4% CO experiment (Figure 1), the same two bands are observed on deposition and increase during annealings. Both bands decrease about $^1/_3$ on mercury arc photolysis, and do not regain their intensities in the following annealing. The 2216.1 cm^{-1} band is assigned to the doubly degenerate C−O stretching mode of $Ag(CO)_3^+$, while 2205.7 cm^{-1} band is due to the triply degenerate C−O stretching mode of $Ag(CO)_4^+$. The $^{13}C^{16}O$ and $^{12}C^{18}O$ isotopic counterparts of these two bands are listed in Table 1. Unfortunately, in the mixed $^{12}CO/^{13}CO$ isotopic experiment, the band splittings cannot be fully resolved because of the dominant absorptions of CO and aggregates around 2140 cm^{-1} and the weak nature of the intermediate bands. Finally, in the 0.01% CCl_4 doped 0.1% CO experiment, the absolute intensities of both $AgCO^+$ and $Ag(CO)_2^+$ bands are tripled while their relative intensity is similar to the 0.1% CO experiment. The $Ag(CO)_3^+$ and $Ag(CO)_4^+$ bands are not observed on deposition, but grow in during successive annealings. After 10 K annealing, both bands are twice as strong as the same bands in 0.1% CO experiment after the same temperature annealing. The CCl_4 molecule efficiently captures electrons, which allows the survival of more Ag^+ cations in these experiments. Hence, the identification of cations is supported by the effect of the CCl_4 additive.

Hurlburt et al. synthesized $[Ag(CO)][B(OTeF_5)_4]$ and $[Ag(CO)_2][B(OTeF_5)_4]$ as crystalline solids when reacting the extremely hygroscopic compounds $AgOTeF_5$, and $AgB(OTeF_5)_4$ with a CO atmosphere.[12] They also reported the antisymmetric C−O stretching mode of $Ag(CO)_2^+$ at 2196−2198 cm^{-1}, and the C−O stretching mode of $AgCO^+$ at 2189−2208 cm^{-1}. Later, the same group identified $Ag(CO)_3^+$ at 2192 cm^{-1} in a similar environment.[13] Our results are in agreement, and the 24−38 cm^{-1} blue shifts in our data are understandable since the counterion and medium constitute a different chemical environment. Similar 18−56 cm^{-1} blue shifts are also observed for $Cu(CO)_n^+$ (n = 1−4).[28]

The DFT calculations of silver carbonyl cations are more straightforward than their neutral counterparts since the cations are closed-shell species. Our calculation indicates that the four silver carbonyl cations $[Ag(CO)_n^+]$ possess $C_{\infty v}$, $D_{\infty h}$, D_{3h} and T_d symmetries with ground states $^1\Sigma^+$, $^1\Sigma_g^+$, $^1A_1'$ and $^1A_1$, when n = 1, 2, 3 and 4, respectively. All four carbonyl cations $[Ag(CO)_n^+$, n = 1−4] are predicted to be more stable than their lower homologues $[Ag(CO)_{n-1}^+$, n = 1−4] and CO. These results can be used to explain the observed annealing behavior of these cations. The sequential dissociation energies (D_0', ZPE and BSSE corrected D_e) of $Ag(CO)_n^+$ (n = 1−4) are deduced from our calculations as 20.3, 22.4, 7.4, 5.7 kcal/mol with B3LYP, and 23.0, 24.9, 7.4, 5.6 kcal/mol with BPW91. Compared to the experimental bond energy data obtained by collision-induced dissociation (21.2 ± 1.2, 26.1 ± 0.9, 13.1 ± 1.8, and 10.8 (+4.4, −0.9) for n = 1−4, respectively),[16] the calculated energies are reasonably good for the mono- and dicarbonyl cations, but somewhat smaller for the tri- and tetracarbonyl cations. Previous MP2 calculations predicted D_0^{298} values of 19.7, 23.8, and 11.3 kcal/mol for $Ag(CO)_n^+$, with n = 1, 2, 3, respectively.[18] The frequencies computed for the carbonyl cations also match the experimental data very well, with scale factors of 0.965, 0.966, 0.967, 0.967 in B3LYP, and 1.005, 1.006, 1.009, 1.009 in BPW91 for $Ag(CO)_n^+$, n = 1, 2, 3 and 4, respectively. The isotopic frequency ratios are listed in Table 5, the general trends are well represented, and not surprisingly, both functionals agree better for these cationic carbonyl calculations than for the neutral species.

$Au(CO)_n^+$ (n = 1−4). Several bands are observed in the higher C−O stretching region on deposition. In the 0.2% CO experiment (Figure 6a−c), the 2236.8 cm^{-1} band is the strongest band on deposition in the 2250−2170 cm^{-1} region, and the 2233.4 and 2203.5 cm^{-1} bands are weaker. A sharp 2194.3 cm^{-1} band belongs to CO^+. In the following annealing cycles, the 2236.8 cm^{-1} band increases about a fourth, the 2233.4 cm^{-1} band almost doubles, the 2203.5 cm^{-1} band more than triples on 8 K annealing, while a new band grows in on the red side of CO^+. These bands are eliminated (or almost eliminated) by full arc photolysis and do not reappear following more annealing. In the 0.4% CO experiment, the same four bands are also observed on deposition (Figure 4). The 2236.8 and 2203.7 cm^{-1} bands have similar intensities on deposition, while the 2233.4 cm^{-1} band is about two-thirds the intensity of the 2236.1 cm^{-1} band. The CO^+ absorption is also observed on deposition, but the band is quite broad and shows evidence of another absorption on its red side. All of those bands grow on annealings, while the feature at 2193.4 cm^{-1} clearly separates itself from the 2194.3 cm^{-1} CO^+ absorption after 10 K annealing (Figure 4c). All of these bands substantially decrease on photolysis, and do not grow following more annealing. The band at 2236.8 cm^{-1} is assigned as the C−O stretching mode of $AuCO^+$, and 2233.3 cm^{-1} is the antisymmetric C−O stretching

mode of $Au(CO)_2^+$, and the 2203.5 and 2193.4 cm^{-1} bands are the doubly degenerate and triply degenerate C−O modes of $Au(CO)_3^+$ and $Au(CO)_4^+$, respectively. The isotopic counterparts of these bands in the ^{13}CO and $C^{18}O$ experiments are listed in Table 2. Only the isotopic counterparts of $Au(CO)_4^+$ cannot be identified due to overlapping by the dominant CO and aggregate absorptions around 2140 cm^{-1}. In the mixed $^{12}CO/^{13}CO$ experiment, the $AuCO^+$ absorption at 2236.8 cm^{-1} gives a doublet feature, while the $Au(CO)_2^+$ absorption shows a 2:3:2 triplet feature with an intermediate band at 2196.1 cm^{-1} (Figure 6g−i). Another very weak feature at 2253.8 cm^{-1} tracks with the triplet and is assigned to the symmetric C−O stretching mode of $Au(^{12}CO)(^{13}CO)^+$. It is worth noting that the interaction of the symmetric and antisymmetric C−O stretching mode in $Au(^{12}CO)(^{13}CO)^+$ molecule is weaker than the silver counterpart which shows a stronger symmetric mode absorption and weaker antisymmetric absorption. Again, in the 0.01% CCl_4 doped experiment, the intensities of all carbonyl cation bands increase by more than half with other experimental conditions keep constant.

Several groups have prepared $AuCO^+$ and $Au(CO)_2^+$ in superacid environments.[14,15] In fluorosulfuric acid, infrared absorptions of $AuCO^+$ and $Au(CO)_2^+$ were reported at 2195 and 2211 cm^{-1}, respectively. In sulfuric acid, the same two cations have absorptions at 2194 and 2208 cm^{-1}. Our neon matrix absorptions are again about 24 and 40 cm^{-1} higher for gold mono- and dicarbonyl cations, respectively, owing to perturbations by the acid media.

DFT calculations performed on gold carbonyl cations show that all four gold carbonyl cations possess the same symmetry as their silver counterparts, namely $C_{\infty v}$, $D_{\infty h}$, D_{3h} and T_d point groups. The frequency calculations yield scale factors: 0.967, 0.968, 0.969, 0.968 for B3LYP, and 1.006, 1.009, 1.012, 1.012 using BPW91 for the C−O stretching modes of $Au(CO)_n^+$, $n = 1-4$, respectively. Although two imaginary modes of $Au(CO)_3^+$ (at −10.5 and −6.7 cm^{-1}), one triply degenerate imaginary mode of $Au(CO)_4^+$ (at −49.2 cm^{-1}) are found with the B3LYP functional, and one triply degenerate mode of $Au(CO)_4^+$ (at −27.3 cm^{-1}) with BPW91, the small magnitudes of these imaginary modes is likely due to the numerical problems in the DFT calculation and the carbonyl frequency calculations are expected to be reliable. Consistent fittings between calculated and experimental vibrational frequencies and similarities between silver and gold carbonyl cations indicate that these calculated electronic states are the ground states observed in the neon matrix. Unfortunately, our DFT/B3LYP calculation gave −1.5 kcal/mol D_0' (ZPE and BSSE corrected) for $Au(CO)_3^+$, but our BPW91 functional found a positive dissociation energy of 0.8 kcal/mol (Table 4). Efforts have been made to search for bound states with lower symmetries; however, all of the converged states have essentially D_{3h} symmetry. A previous MP2 calculation predicted 8.5 (D_e) and 7.3 kcal/mol (D_0^{298}) for the same D_{3h} symmetry $^1A_1'$ ground-state $Au(CO)_3^+$, with no negative modes.[18] Contrasting results in different calculations clearly show the difficulty for gold compounds, which have a strong relativistic effect.[23]

Comparison of Cu, Ag, and Au Carbonyls. Compared to the copper and CO system, the products with silver, gold and CO are quite different. In copper experiments, both metal carbonyl cation and anion species have been observed in addition to neutral carbonyls.[28] However, no evidence for carbonyl anions is found in silver and gold experiments, while the same $(CO)_2^-$ absorption signifies the presence of electrons in all three systems. The bonding in metal carbonyls is classically explained by the σ donation and π back-donation model. The 5σ electron of the CO molecule donates to the metal valence σ-symmetry orbital, while the metal d_π electron back-donates to the $2\pi^*$ orbital of CO. If a metal atom (or ion) has the ns^2 valence electronic configuration, σ donation bonding is blocked since repulsion between the filled metal s orbital and CO 5σ orbital is enormous. It is energy-wise for the metal to promote an s electron into a vacant d orbital and form two sd hybridized orbitals, then one sd orbital can be used to form a σ bond. In the copper group anions with $d^{10}s^2$ configurations, the above s → d promotion is not possible so s → p promotion and hybridization instead take place. The energy difference between s and p orbitals however is larger than the energy difference between s and d orbitals as it is generally true that metal carbonyl anions are harder to form than cations and neutrals. For gold, a very large relativistic effect[44] takes place, and the contracted 6s orbital makes the energy difference between s and p orbitals very large. As a consequence, energy gains in the formation of metal−carbonyl bonds are essentially not large enough to compensate energy costs to promote electrons into gold p orbitals, and hence gold carbonyl anions are not observed. On the other hand, although the energy difference between s and p orbitals in silver and copper atoms are similar, an extra electron in AgCO (which is not a bona fide compound) will make a weak bond even weaker. Efforts were made to search for bound states of silver and gold monocarbonyl anions, but no bound states were found in our DFT calculations. A previous MP4 calculation for $AgCO^-$ also failed to find a bound state.[21]

In neutral carbonyl systems, only silver di- and tricarbonyl, and gold mono- and dicarbonyl are found, while all three copper carbonyls have been observed. Again, the bonding can be understood based on the energy differences between valence orbitals of the three metal atoms. In the monocarbonyl systems, the back-donation occurs from metal d_π orbital. Since the valence d_π orbital in silver is extremely stable compared to the same orbitals in copper and gold atoms, the π back-donation bonding in silver is not efficient. The absence of silver monocarbonyl in our neon matrix study is due to the weak bonding interaction between silver atom and CO molecule. In the D_{3h} symmetry tricarbonyl system, p orbitals involve in the π back-bonding in a great deal. Because of the strong relativistic effect in gold atom, the energy difference between gold 6s and 6p orbitals is much larger than that of the two corresponding orbitals in copper and silver atoms. A higher s−p promotion energy makes gold tricarbonyl an unstable molecule, which is also described by our DFT calculation.

Metal carbonyl cations are observed for all three metals, and their spectra are extremely similar while all C−O stretching frequencies are higher than the free C−O stretching frequency. The bonding in such nonclassical carbonyls has been described in several previous papers, and an electrostatic bonding model has been proposed.[17] In our experiment, the fairly close C−O stretching frequencies (2234.4, 2233.1, and 2236.8 cm^{-1} in Cu, Ag, and Au monocarbonyl cations, respectively) support electrostatic bonding. Strauss has recently discussed the nonclassical behavior in silver and copper carbonyl cations.[45] A weaker Ag^+−CO bond (smaller D_e value for $AgCO^+$) than Cu^+−CO is explained as a result of the larger energy difference between valence s and d_σ orbitals which causes a longer Ag^+−CO bond and hence weaker π back-donation bonding. To expand this explanation to gold, relativistic effects play an important role once again, which reduces the energy difference between 6s and 5d orbitals and consequently makes Au^+−CO a stronger bond.

V. Conclusions

Laser-ablated Ag and Au atoms and cations have been reacted with CO molecules during condensation in a neon matrix at 4 K. Through annealing, photolysis, CO concentration variation and isotopic substitution experiments, metal carbonyl cations $[M(CO)_n^+$ (M = Ag, Au; $n = 1-4)]$, as well as neutrals $[Ag(CO)_n$, $(n = 2, 3)$; $Au(CO)_n$, $(n = 1, 2)$; $Au_2(CO)_2]$ are identified. Doping with the electron trapping molecule CCl_4 confirms identification of the cationic species.

DFT calculations (B3LYP and BPW91 functionals) have been performed for all products, and good agreement has been found with the experimental results. Overall, as closed-shell systems, carbonyl cations give better agreement, while neutral carbonyls are more theoretically difficult as open-shell systems. The average scale factors for the C−O vibrational modes in metal carbonyls are 0.968 ± 0.014 (B3LYP) and 1.007 ± 0.016 (BPW91).

The difference between Cu, Ag, and Au carbonyls are explained by the classical σ donation and π back-donation bonding scheme of metal carbonyls. The energy differences between the metal valence d, s, and p orbitals are the main reasons for different metal carbonyls in the Cu, Ag, and Au systems.

Acknowledgment. The authors gratefully acknowledge National Science Foundation and Petroleum Research Fund support.

References and Notes

(1) Mond, L.; Langer, C.; Quincke, F. *J. Chem. Soc.* **1890**, 749. Mond, L.; Langer, C. *J. Chem. Soc.* **1891**, 1090.

(2) Cotton, F. A.; Wilkinson, G. *Advanced Inorganic Chemistry*, 5th ed.; Wiley: New York, 1988. Collman, J. P.; Hegedus, L. S.; Norton, J. R.; Finke, R. G. *Principles and Applications of Organotransition Metal Chemistry*; University Science Books: Mill Vally, CA, 1987.

(3) Tolman, C. A. *Chem. Soc. Rev.* **1972**, *1*, 337. Casey, C. P.; Cyr, C. R. *J. Am. Chem. Soc.* **1973**, *95*, 2248. Mitchener, J. C.; Wrighton, M. S. *J. Am. Chem. Soc.* **1981**, *103*, 975. Whetten, R. L.; Fu, K.; Grant, E. R. *J. Am. Chem. Soc.* **1982,** *104*, 4270. Weitz, E. *J. Phys. Chem.* **1987**, *91*, 3945. Vannice, M. A. *Catal. Today* **1992**, *12*, 255.

(4) Walsh, S. P.; Goddard, W. A., III. *J. Am. Chem. Soc.* **1976**, *98*, 7908.

(5) Nekrylova, J. V.; Harrison, I. *J. Chem. Phys.* **1994**, *101*, 1730.

(6) Ogden, J. S. *Chem. Commun.* **1971**, 978. Froben, F. W.; Rabin, I.; Ritz, M.; Schulze, W. *Z. Phys. D* **1996**, *38*, 335.

(7) McIntosh, D.; Ozin, G. A. *J. Am. Chem. Soc.* **1976**, *98*, 3167.

(8) McIntosh, D.; Ozin, G. A. *Inorg. Chem.* **1977**, *16*, 51.

(9) Kasai, P. H.; Jones, P. M. *J. Phys. Chem.* **1985**, *89*, 1147.

(10) Kasai, P. H.; Jones, P. M. *J. Am. Chem. Soc.* **1985**, *107*, 6385.

(11) Chenier, J. H. B.; Hampson, C. A.; Howard, J. A.; Mile, B. *J. Phys. Chem.* **1988**, 92, 2745.

(12) Hurlburt, P. K.; Anderson, O. P.; Strauss, S. H. *J. Am. Chem. Soc.* **1991**, *113*, 6277. Hurlburt, P. K.; Rack, J. J.; Dec, S. F.; Anderson, O. P.; Strauss, S. H. *Inorg. Chem.* **1993**, *32*, 373. Hurlburt, P. K.; Rack, J. J.; Luck, J. S.; Dec, S. F.; Webb, J. D.; Anderson, O. P.; Strauss, S. H. *J. Am. Chem. Soc.* **1994**, *116*, 10003.

(13) Rack, J. J.; Moasser, B.; Gargulak, J. D.; Gladfelter, W. L.; Hochheimer, H. D.; Strauss, S. H. *J. Chem. Soc., Chem. Commun.* **1994**, 685. Rack, J. J.; Polyakov, O. G.; Gaudinski, C. M.; Hammel, J. W.; Kasperbauer, P.; Hochheimer, H. D.; Strauss, S. H. *Appl. Spectrosc.*, **1998**, *52*, 1035.

(14) Willner, H.; Aubke, F. *Inorg. Chem.* **1990**, *29*, 2195. Willner, H.; Schaebs, J.; Hwang, G.; Mistry, F.; Jones, R.; Trotter, J.; Aubke, F. *J. Am. Chem. Soc.* **1992**, *114*, 8972.

(15) Xu, Q.; Imamura, Y.; Fujiwara, M.; Souma, Y. *J. Org. Chem.* **1997**, *62*, 1594.

(16) Meyer, F.; Chen, Y.; Armentrout, P. B. *J. Am. Chem. Soc.* **1995**, *117*, 4071.

(17) Barnes, L. A.; Rosi, M.; Bauschlicher, C. W., Jr. *J. Chem. Phys.* **1990**, *93*, 609.

(18) Veldkamp, A.; Frenking, G. *Organometallics* **1993**, *12*, 4613.

(19) Dargel, T. K.; Hertwig, R. H.; Koch, W.; Horn, H. *J. Chem. Phys.* **1998**, *108*, 3876.

(20) Jonas, V.; Thiel, W. *J. Phys. Chem. A* **1999**, *103*, 1381.

(21) Watanabe, K.; Nagashima, U.; Hosoya, H. *Chem. Phys. Lett.* **1993**, *209*, 109.

(22) Marian, C. M. *Chem. Phys. Lett.* **1993**, *215*, 582.

(23) Schwerdtfeger, P.; Bowmaker, G. A. *J. Chem. Phys.* **1994**, *100*, 4487.

(24) Bondybey, V. E.; Smith, A. M.; Agreiter, J. *Chem. Rev.* **1996**, *96*, 2113.

(25) Zhou, M. F.; Andrews, L. *J. Am. Chem. Soc.* **1998**, *120*, 11499 (Ni + CO).

(26) Zhou, M. F.; Andrews, L. *J. Chem. Phys.* **1999**, *110*, 6820 ($C_2O_4^+$).

(27) Liang, B.; Zhou, M. F.; Andrews, L. *J. Phys. Chem.* **2000**, *104*, 3905 (Ni, Pd, Pt + CO in Ne).

(28) Zhou, M. F.; Andrews, L. *J. Chem. Phys.* **1999**, *111*, 4548 (Cu + CO in Ne).

(29) Zhou, M. F.; Andrews, L. *J. Phys. Chem. A* **1999**, *103*, 7773 (Co, Rh, Ir + CO in Ne).

(30) Burkholder, T. R.; Andrews, L. *J. Chem. Phys.* **1991**, *95*, 8697.

(31) Hassanzadeh, P.; Andrews, L. *J. Phys. Chem.* **1992**, *96*, 9177.

(32) Chertihin, G. V.; Andrews, L. *J. Phys. Chem.* **1995**, *99*, 6356.

(33) Krim, L.; Manceron, L.; Alikhani, M. E. *J. Phys. Chem. A* **1999**, *103*, 2592.

(34) Frisch, M. J.; Trucks, G. W.; Schlegel, H. B.; Gill, P. M. W.; Johnson, B. G.; Robb, M. A.; Cheeseman, J. R.; Keith, T. A.; Petersson, G. A.; Montgomery, J. A.; Raghavachari, K.; Al-Laham, M. A.; Zakrzewski, V. G.; Ortiz, J. V.; Foresman, J. B.; Cioslowki, J.; Stefanov, B. B.; Nanayakkara, A.; Challacombe, M.; Peng, C. Y.; Ayala, P. Y.; Chen, W.; Wong, M. W.; Andres, J. L.; Replogle, E. S.; Gomperts, R.; Martin, R, L.; Fox, D. J.; Binkley, J. S.; Defrees, D. J.; Baker, J.; Stewart, J. P.; Head-Gordon, M.; Gonzalez, C.; Pople, J. A. *Gaussian 94*, Revision B.1; Gaussian Inc.: Pittsburgh, PA, 1995.

(35) Perdew, J. P.; Wang, Y. *Phys. Rev. B* **1992**, *45*, 13244.

(36) Lee, C.; Yang, E.; Parr, R. G. *Phys. Rev. B* **1988**, *37*, 785.

(37) McLean, A. D.; Chandler, G. S. *J. Chem. Phys.* **1980**, *72*, 5639. Wachters, A. J. H. *J. Chem. Phys.* **1970**, *52*, 1033. Hay, P. J. *J. Chem. Phys.* **1977**, *66*, 4377. Raghavachari, K.; Trucks, G. W. *J. Chem. Phys.* **1989**, *91*, 1062.

(38) Hay, P. J.; Wadt, W. R. *J. Chem. Phys.* **1985**, *82*, 270. Wadt, W. R.; Hay, P. J. *J. Chem. Phys.* **1985**, *82*, 284. Hay, P. J.; Wadt, W. R. *J. Chem. Phys.* **1985**, *82*, 299.

(39) Boys, S. F.; Bernardi, F. *Mol. Phys.* **1970**, *19*, 553.

(40) Adamo, C.; Lelj, F. *J. Chem. Phys.* **1995**, *103*, 10605.

(41) Thompson, W. E.; Jacox, M. E. *J. Chem. Phys.* **1991**, *95*, 735.

(42) Darling, J. H.; Ogden, J. S. *J. Chem. Soc., Dalton Trans.* **1972**, 2496.

(43) Bytheway, I.; Wong, M. W. *Chem. Phys. Lett.* **1998**, *282*, 219.

(44) Pyykkö, P. *Chem. Rev.* **1988**, *88*, 563.

(45) Strauss, S. H. *J. Chem. Soc., Dalton Trans.* **2000**, 1.